A green and environmentally benign route to synthesizing Z-scheme Bi_2S_3-TCN photocatalyst for efficient hydrogen production

Lang Yuan[1,2†], Yihang Yin[2†], Peng Xiang[2], Yugui Shao[2], Jie Gao[2], Jianan Liu[2], Huiyuan Meng[2,3], Li Li[1,2]*, Ying Xie[2]*, Xudong Xiao[2]* and Baojiang Jiang[2]

[1]College of Modern Agriculture and Ecological Environment, Heilongjiang University, Harbin, China, [2]Heilongjiang Provincial Key Laboratory of Environmental Nanotechnology, School of Chemistry and Materials Science, Heilongjiang University, Harbin, China, [3]School of Safety Engineering, Heilongjiang University of Science and Technology, Harbin, Heilongjiang, China

Designing and developing photocatalysts with excellent performance in order to achieve efficient hydrogen production is an important strategy for addressing future energy and environmental challenges. Traditional single-phase photocatalytic materials either have a large bandgap and low visible light response or experience rapid recombination of the photogenerated carriers with low quantum efficiency, seriously hindering their photocatalytic applications. To solve these issues, an important solution is to construct well-matched heterojunctions with highly efficient charge separation capabilities. To this end, an *in situ* sulfurization reaction was adopted after the deposition of Bi^{3+} supramolecular complex on a layered supramolecular precursor of tubular carbon nitride (TCN). X-ray diffraction (XRD) patterns confirmed that the as-prepared sample has a good crystalline structure without any other impurities, while high-resolution transmission electron microscopy (HR-TEM) revealed that the heterojunction possesses a 2D structure with a layer of nano-array on its surface. Combined Fourier-transform infrared (FT-IR) spectra and energy-dispersive X-ray spectroscopy (EDX) revealed the interfacial interactions. Owing to the formation of the Z-scheme heterojunction, the visible light adsorption and the separation efficiency of the photo-generated carriers are both obviously enhanced, leaving the high energy electrons and high oxidative holes to participate in the photocatalytic reactions. As a result, the photocatalytic hydrogen evolution rate of Bi_2S_3-TCN achieves 65.2 $\mu mol \cdot g^{-1} \cdot h^{-1}$. This proposed green and environmentally benign route can also be applied to construct other sulfides with 2D TCN, providing some important information for the design and optimization of novel carbon-nitride-based semiconductors.

KEYWORDS

photocatalytic, heterojunction, TCN, Bi_2S_3, semiconductor

1 Introduction

The application of photocatalytic technology to produce hydrogen is an important means of addressing energy and environmental issues, with significant implications for achieving carbon neutrality and a benign carbon cycle. As a semiconductor, tubular carbon nitride (TCN) is widely used in photocatalysis due to its excellent thermodynamic stability, suitable band gap (~2.7 eV), high surface area, and low cost (Cao et al., 2015; Cheng et al., 2021). However, as with traditional semiconductors, single-phase g-C_3N_4 exhibits low mobility of photogenerated electrons and holes under light radiation, leading to high recombination rates of charge carriers and low quantum efficiency (Thomas et al., 2008; Kumar et al., 2013). Additionally, TCN requires high light excitation energy, and it can only absorb and utilize ultraviolet and a narrow range of visible light less than 460 nm, resulting in unsatisfactory photocatalytic performance (Chen et al., 2014).

To address these issues, researchers have employed methods such as atomic-level doping (Zhang et al., 2011a; Pan et al., 2011), surface chemistry via molecular-level modification (Zhang et al., 2010; Chu et al., 2013), and construction of heterojunctions (Huang et al., 2022; Lei et al., 2022; Wang et al., 2022) to enhance the photocatalytic activity of TCN. Furthermore, the 2D layered structure and polymeric nature of TCN make it a very suitable host for constructing heterojunctions with various inorganic materials (Cheng et al., 2021). Therefore, choosing an appropriate semiconductor to form a desired composite with TCN has become an important strategy for developing inexpensive and efficient photocatalysts. Compared to metal oxides, metal sulfides usually have smaller band gaps, giving them superior visible light activity (Zhu et al., 2022). Sulfides such as CdS, ZnS, CuS, and $Cd_xZn_{1-x}S$ have been widely used as photocatalysts for hydrogen production due to their tunable band gaps and excellent visible light utilization (Zhang et al., 2011b; Li et al., 2013; Yuan et al., 2018). As a member of the sulfide family, Bi_2S_3 has a band gap of ~1.3–1.7 eV (Chen et al., 2017; Liu et al., 2019) and also exhibits excellent visible light activity. When combined with other wide-bandgap semiconductors, Bi_2S_3 as a photosensitizer can effectively improve the photocatalytic performance of the composite (Chen et al., 2017). Moreover, non-toxic Bi_2S_3 has a layered structure, allowing it to easily form heterojunctions with 2D-structured TCN through surface chemical modification, which have been applied in the degradation of dyes and pollutants (Zhou et al., 2015; Chen et al., 2017; Yin et al., 2018; Hu et al., 2019; Liu et al., 2019; Gu et al., 2021; Okab and Alwared, 2023) and the reduction of CO_2 (Guo et al., 2020), as well as efficiently killing multidrug-resistant bacteria (Li et al., 2019).

Although Bi_2S_3-TCN has some applications in the above fields, there are significant differences in the photocatalytic mechanisms reported, and its application in the field of photocatalytic hydrogen production is also rather limited (Li et al., 2023). To reveal the nature of interface interactions and the relevant photocatalytic mechanisms, this study employed a green and environmentally benign route to synthesize a Z-scheme Bi_2S_3-TCN heterojunction photocatalysts. The results indicate that the formation of a heterojunction interface promotes an obvious charge transfer between the two components, enhancing the separation efficiency of charge carriers. The interface interaction also helps further stabilize the crystal structure of Bi_2S_3, thus significantly expanding the visible light absorption capability of the heterojunction while inhibiting the photo-corrosion of sulfides. In addition, the Z-scheme band alignment ensures the reduction and oxidation capabilities of photogenerated electrons and holes respectively, synergistically leading to outstanding and stable photocatalytic hydrogen production.

2 Experimental section

2.1 Preparation of the samples

Synthesis of the supramolecular precursors and TCN. We dissolved 1.2 g of melamine in 75 mL of deionized water and stirred for 30 min; then 1.44 g of solid phosphorous acid was added with continuous stirring for another 60 min. The mixture was transferred into an autoclave lined with Teflon and kept at 180°C for 10 h. Finally, the product was filtered and washed ten times with deionized water. After drying at 60°C, the samples were placed in a magnetic boat and calcined at 450°C in a tube furnace for 2 h to obtain TCN.

Synthesis of Bi_2S_3. We uniformly dispersed 0.001 mol $Bi(NO_3)_3 \cdot 5H_2O$ in 40 mL anhydrous ethanol and stirred for 2 h. After the hydrolysis of the precursor, the product was filtered and washed with ethanol three times and then dried at 60°C. Sublimed sulfur and the product were put into two magnetic boats, which were then transferred in the tube furnace and heated to 450°C with a heating rate of 2.5°C/min. After calcination for 2 h in an argon atmosphere, a Bi_2S_3 sample was obtained.

Synthesis of Bi_2S_3-TCN. We used 0.001 mol of $Bi(NO_3)_3 \cdot 5H_2O$ as a Bi source to grow a Bi^{3+} supramolecular complex *in situ* on the surface of the layered supramolecular precursor of TCN (4 g) with anhydrous ethanol as solvent. After stirring for 2 h, the product was thrice filtered and washed with ethanol and dried at 60°C. Sublimed sulfur was then introduced as a sulfur source to vulcanize the precursor via vapor deposition calcination. Unlike the traditional hydrothermal preparation method, the growth of the Bi-based molecular complex on the 2D surface of TCN precursors not only guaranteed close interface contact between the two components but also reduced the reaction step, accompanied by an improved reaction yield and obviously reduced consumption of the organic chemical reagents. This synthetic method can effectively avoid the production of pollution and the waste of resources as far as possible and thus become a green and environmentally benign route.

2.2 Structural characterizations and photocatalytic tests

X-ray diffraction (XRD) patterns were obtained by a Bruker D8 diffractometer using Cu Kα radiation, while the Fourier transform infrared spectroscopy (DT-IR) data were recorded using the KBr pellets on a PerkinElmer Spectrum One spectrometer. The microstructures were identified by scanning electron microscopy (SEM, FEI Sirion 200) and transmission electron microscopy (FEI Talos F200S). Optical absorption and
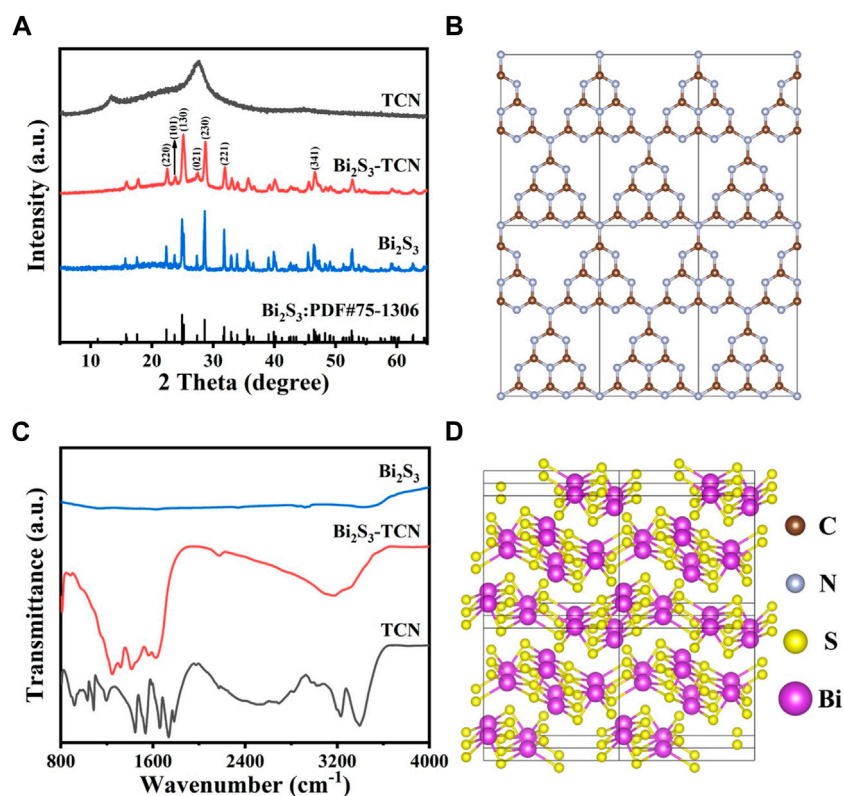
FIGURE 1
(A) XRD pattern for TCN, Bi_2S_3, and Bi_2S_3-TCN samples. **(B)** Crystal structures of TCN. **(C)** FT-IR spectrum for TCN, Bi_2S_3, and Bi_2S_3-TCN samples. **(D)** Crystal structures of Bi_2S_3.

diffuse reflectance spectrometry (UV-DRS) were performed using a UV-Vis spectrophotometer (Lambda 950). The work function of samples was tested by Scanning Kelvin probe (SKP) (SKP5050 system, Scotland). The photoelectrochemical measurements were performed on a Princeton Versa STAT 2 electrochemical workstation with a standard three-electrode system (Ag/AgCl electrode reference electrode and Pt foil counter electrode). The relevant testing was conducted for the Mott–Schottky curves under natural light exposure with 0.5 M Na_2SO_4 as the electrolyte.

The photocatalytic hydrogen production experiments were performed in a photocatalytic hydrogen production system (Labsolar-6A, Beijing Perfect Light Technology Co., Ltd.). A cut-off filter ($\lambda > 400$ nm) was used to remove the UV light to produce visible light, and a 300 W Xe lamp was used as the light source. In a typical photocatalytic test, 50 mg of photocatalyst was dispersed in 100 mL of an aqueous solution containing 10 mL of lactic acid and 90 mL of water as the sacrificial reagent; the solution was stirred continuously during the test. Before visible light irradiation, the opening was sealed with a quartz cap with a silicone rubber gasket, and the test apparatus was evacuated for 30 min to remove O_2 from the reaction system. Finally, the mixture was exposed under radiation and the gas product was analyzed using a gas chromatograph (Techcomp 7900, TCD, Ar carrier) to determine hydrogen production. The hydrogen production rate was calculated using the method of normalization of catalyst dosage and time.

3 Results and discussion

To determine the crystalline structure, XRD patterns of different samples are presented in Figure 1A. The results indicate that TCN exhibits two diffraction peaks at approximately 13.0° and 28.0°, corresponding to the (100) and (002) crystal planes of graphitic carbon nitride (Li et al., 2022). The former primarily originates from the ordered repetitive arrangement of the in-plane tris-S-triazine structure of TCN (Figure 1B), while the latter is associated with the characteristic stacking of conjugated aromatic groups (Li et al., 2021; Sarkar et al., 2022). XRD peaks are sharp and clear for Bi_2S_3, indicating a good crystalline property. The diffraction peaks at 22.5°, 23.9°, 25.2°, 27.7°, 28.7°, 31.9°, and 46.7° correspond to (220), (101), (130), (021), (230), (221), and (341), and the crystal structure belongs to the orthorhombic system with a space group of P_{nma}, which is consistent with the data in the standard card (PDF#75-1360, Figure 1A) (Lee et al., 2018; Sun et al., 2020). In addition, the diffraction peaks of both Bi_2S_3 and TCN are simultaneously observed in the Bi_2S_3-TCN sample, while the (002) diffraction peak of TCN and the (021) peak of Bi_2S_3 obviously overlap, resulting in a significant change of the intensities nearby. This demonstrates the coexistence of the two components in the composite and the successful construction of the Bi_2S_3-TCN heterojunction. The absence of XRD patterns for other impurities indicates the high purity of Bi_2S_3-TCN.

To reveal the impact of the introduction of Bi_2S_3 on the structure of TCN, Fourier-transform infrared (FT-IR) spectra of different samples are presented in Figure 1C. Corresponding to the building blocks in
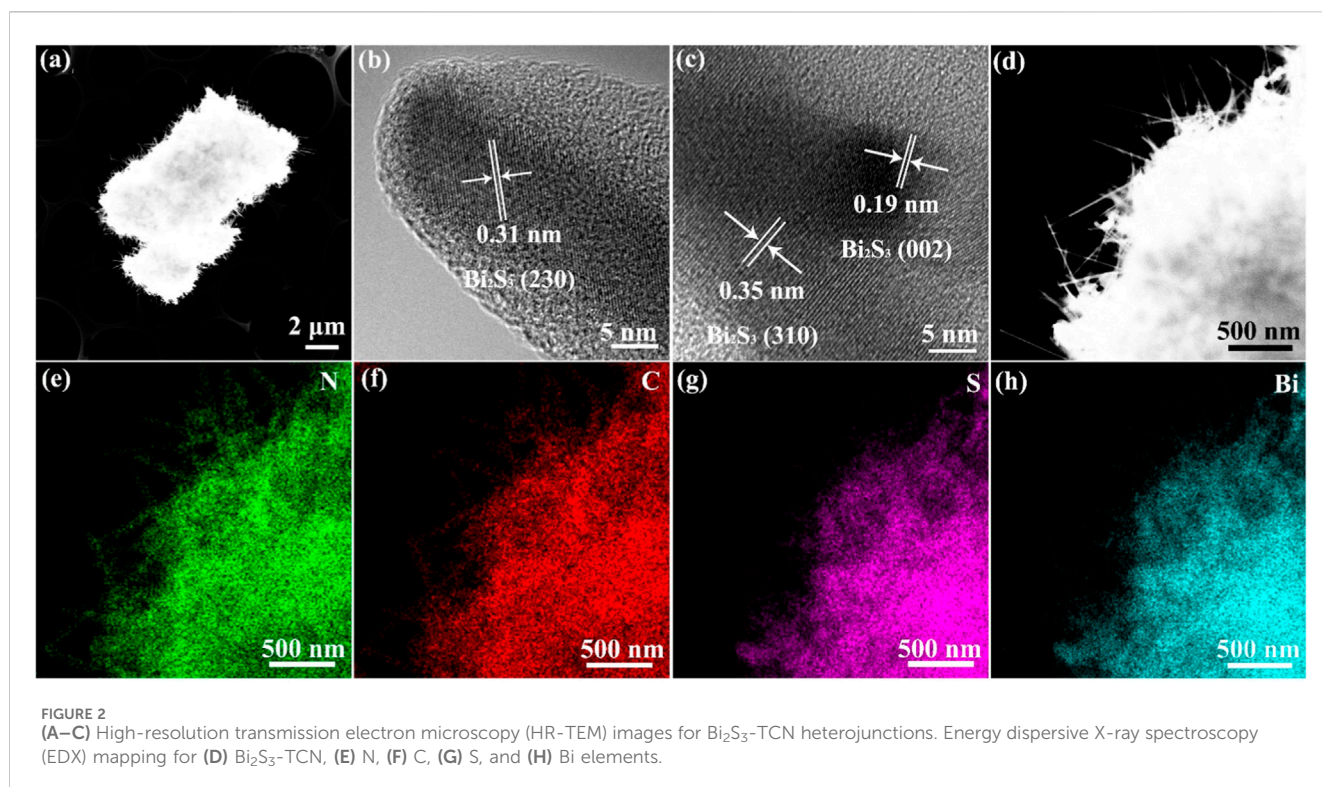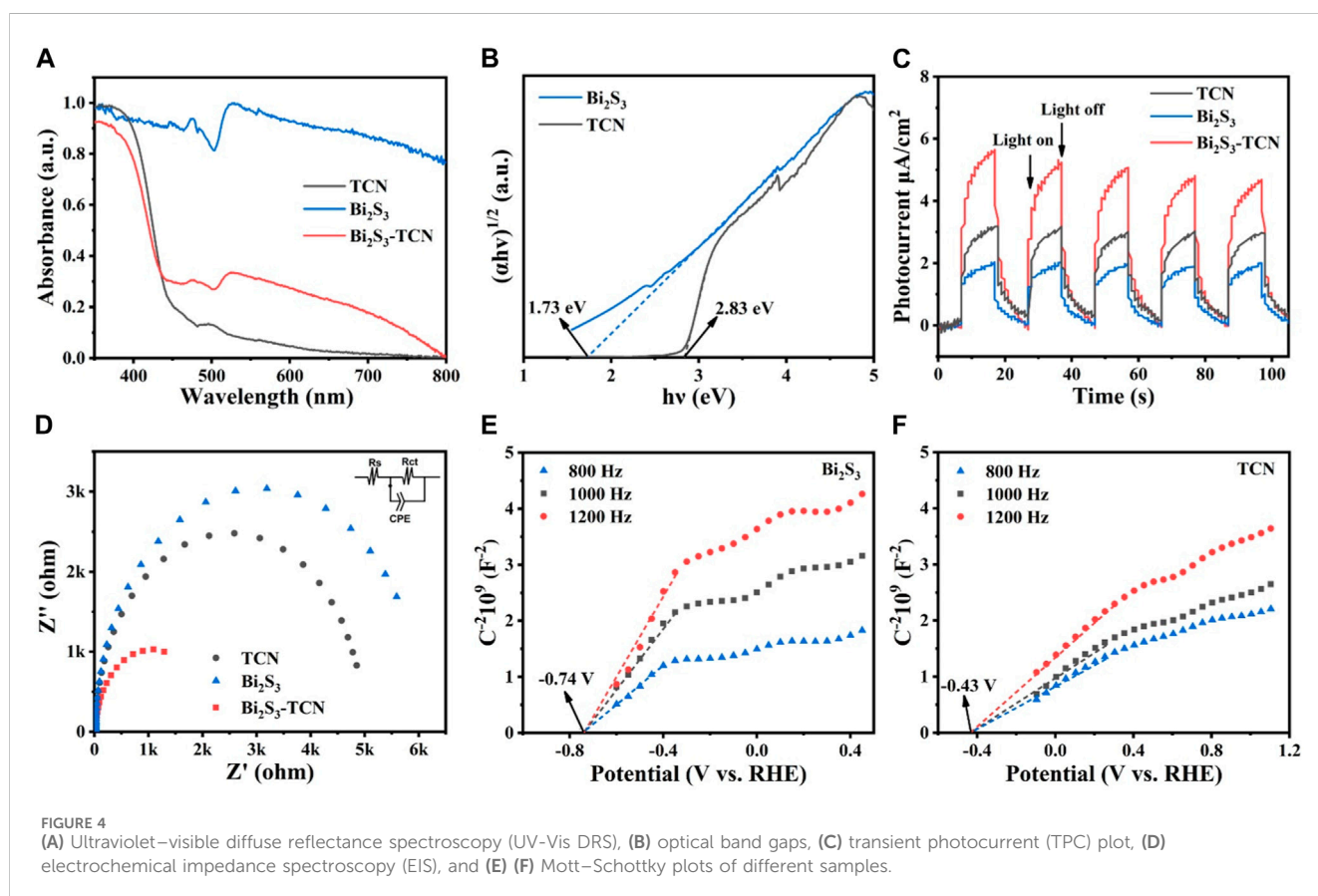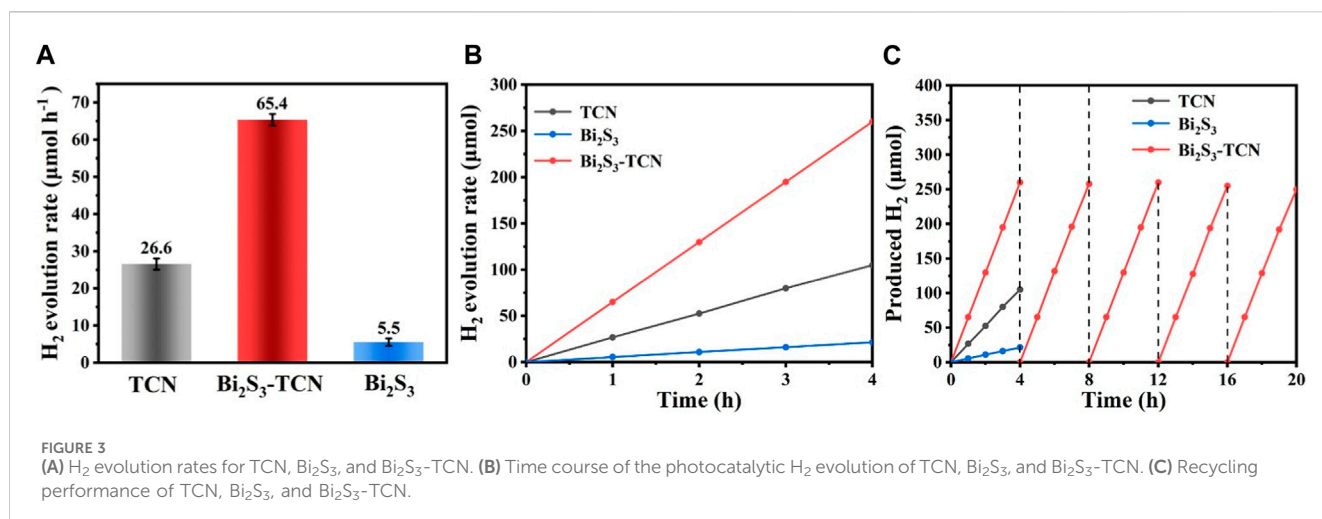
FIGURE 2
(A–C) High-resolution transmission electron microscopy (HR-TEM) images for Bi_2S_3-TCN heterojunctions. Energy dispersive X-ray spectroscopy (EDX) mapping for **(D)** Bi_2S_3-TCN, **(E)** N, **(F)** C, **(G)** S, and **(H)** Bi elements.

Figure 1B (Xiao et al., 2021), TCN exhibits a series of absorption bands (Yin et al., 2018): the absorption peak near 810 cm^{-1} corresponds to the stretching vibration of the triazine ring; the fingerprint signals within the range of 1,100–1,700 cm^{-1} correspond to the stretching vibrations of the C-N aromatic hetero-rings; the broad absorption band in the range of 3,000–3,600 cm^{-1} is mainly attributed to the stretching modes of primary and secondary amines, as well as the O–H stretching vibration of surface-adsorbed water and intermolecular hydrogen bonding interactions. Thanks to the layered structure of Bi_2S_3 (Figure 1D), its introduction may lead to the formation of heterojunctions with the TCN through interfacial interactions. This causes a slight shift of the above IR characteristic peaks toward lower wave numbers. However, there is no significant difference in the intensity of absorption peaks in the sample compared to the pristine TCN samples. The layered structure of TCN in the heterojunctions is therefore not destroyed by the introduction of Bi_2S_3, indicating good structural integrity for Bi_2S_3-TCN.

Figure 2A shows the high-resolution electron microscopy (HR-TEM) images and elemental distribution maps of the Bi_2S_3-TCN heterojunction. The results clearly show that the Bi_2S_3-TCN has a layered structure with special morphology. After assembly of the Bi^{3+} supramolecular complex on the TCN precursor surface, an *in situ* sulfurization process occurs and results in the formation of a layer of nano-array structures on the heterojunction surface. This effectively enhances the specific surface area and the number of active sites of the composite while simultaneously reducing the diffusion distance of photogenerated charge carriers. This is highly favorable for improving photocatalytic activity. In addition, the test results in Figures 2B,C further clarify that the crystal planes with the interplanar distances of 0.31 nm, 0.19 nm, and 0.35 nm belong to the Bi_2S_3 (230), (002), and (310) crystalline planes, respectively (Kumar et al., 2021). The EDX mapping further demonstrates a uniform distribution of the four elements (N, C, S, and Bi) throughout the whole selected region (Figures 2D–H). These features suggest that a well-contacted interface is formed between Bi_2S_3 and TCN in the heterojunction. Therefore, it can be anticipated that this heterojunction with a unique surface morphology and 2D structure will exhibit excellent photocatalytic performance.

The photocatalytic hydrogen production experiment was applied to evaluate the photocatalytic activity of the catalyst (Li et al., 2023). The hydrogen evolution rate of Bi_2S_3-TCN is 65.2 µmol h^{-1}, which is 2.43 times that of TCN (26.8 µmol h^{-1}) and 11.64 times that of Bi_2S_3 (5.6 µmol h^{-1}). The mean values of the multiple experiments were Bi_2S_3-TCN (65.4 µmol h^{-1}), TCN (26.6 µmol h^{-1}), and Bi_2S_3 (5.5 µmol h^{-1}), respectively (Figure 3A). As shown in Supplementary Table S1, the hydrogen evolution performance of Bi_2S_3-TCN was compared with existing heterojunction photocatalytic materials, demonstrating that Bi_2S_3-TCN had better photocatalytic hydrogen evolution activity. The significant increase in hydrogen production rate demonstrates that the formation of Bi_2S_3-TCN Z-scheme heterostructure provides a new charge transfer pathway with great advantages in photocatalytic reactions. At the same time, Bi_2S_3-TCN maintained a stable H$_2$ yield during the 4-h test period (Figure 3B). The durability of Bi_2S_3-TCN was tested over five repeated cycles (Figure 3C). After 20 h of continuous testing, Bi_2S_3-TCN still maintained original photocatalytic activity, indicating that its heterojunction photocatalyst has excellent photostability. This indicates that the Bi_2S_3 and TCN heterojunction photocatalyst prepared can promote rapid separation and transfer of charge under light radiation while maintaining the stability of structure and morphology due to its tight heterogeneous structure.

FIGURE 3
(A) H$_2$ evolution rates for TCN, Bi$_2$S$_3$, and Bi$_2$S$_3$-TCN. **(B)** Time course of the photocatalytic H$_2$ evolution of TCN, Bi$_2$S$_3$, and Bi$_2$S$_3$-TCN. **(C)** Recycling performance of TCN, Bi$_2$S$_3$, and Bi$_2$S$_3$-TCN.

FIGURE 4
(A) Ultraviolet−visible diffuse reflectance spectroscopy (UV-Vis DRS), **(B)** optical band gaps, **(C)** transient photocurrent (TPC) plot, **(D)** electrochemical impedance spectroscopy (EIS), and **(E) (F)** Mott−Schottky plots of different samples.

To reveal the origin of the photocatalytic performance, UV-Vis DRS (Figure 4A) was used (Mua et al., 2021). It can be seen clearly that the absorption edge of TCN is close to 460 nm, while that of Bi$_2$S$_3$ extends significantly to 700 nm, indicating that Bi$_2$S$_3$ has much better visible light response. Compared with pristine TCN, the introduction of Bi$_2$S$_3$ leads to a red-shifted adsorption edge for the heterojunction. The interfacial interactions formed between TCN and Bi$_2$S$_3$ can modulate the positions of the valence band (VB) and conduction band (CB), obviously reducing the calculated band gap of Bi$_2$S$_3$-TCN (Figure 4B).

Consequently, Bi$_2$S$_3$-TCN shows much stronger absorption of visible light, which is favorable for subsequent photocatalytic reactions. In addition to the above characteristics, the TPC plot in Figure 4C further identifies that the photocurrent of Bi$_2$S$_3$-TCN under visible light radiation is much higher than those of TCN and Bi$_2$S$_3$, and that even Bi$_2$S$_3$ possesses the smallest band gaps (Hao et al., 2020). This indicates that the intimate interface formed between the two components does facilitate the separation of the photocatalytic electrons and holes, leading to a much higher charge separation efficiency. Such a result can be
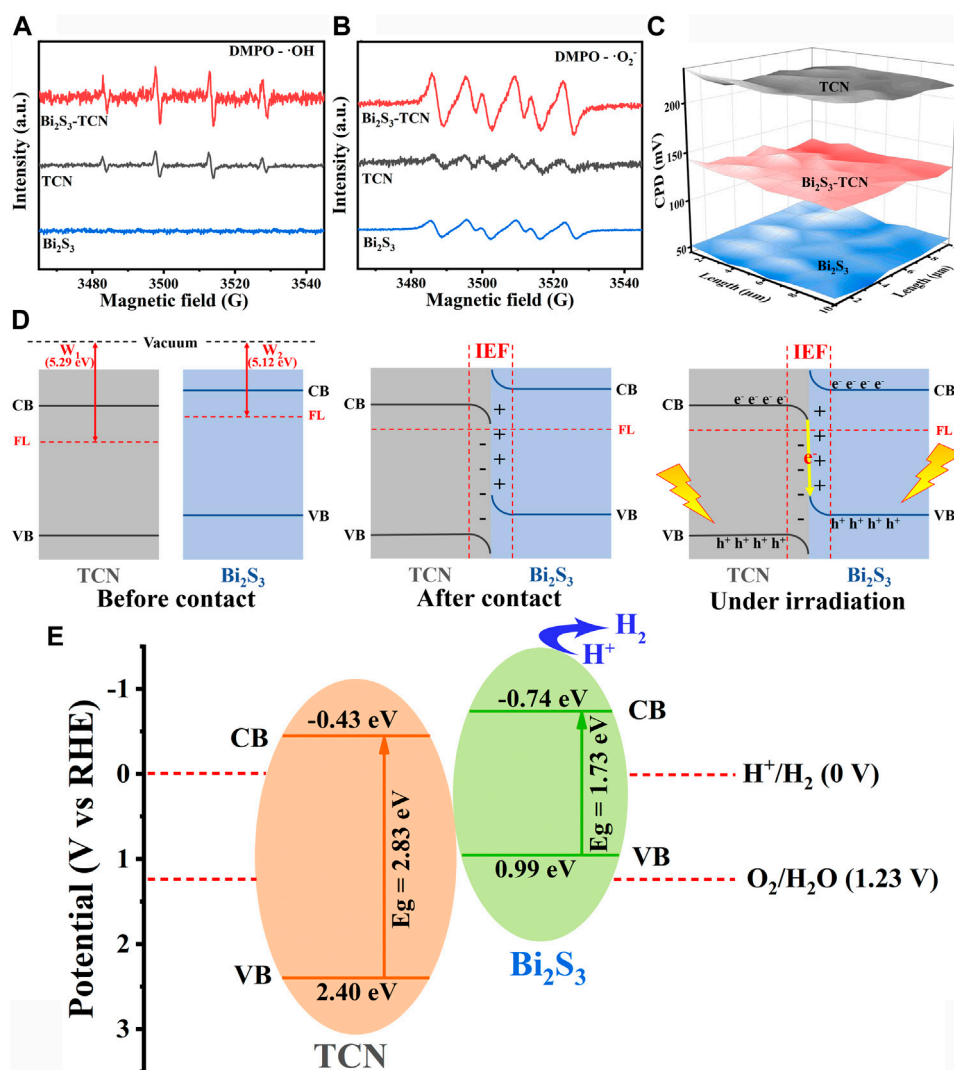
FIGURE 5
(A, B) ESR spectra of TCN, Bi_2S_3, and Bi_2S_3-TCN under visible-light illumination. (C) Relative WF maps of TCN, Bi_2S_3, and Bi_2S_3-TCN. (D) Energy band diagrams of TCN and Bi_2S_3 before and after contact, BIEF formation, and charge transfer processes in Z-scheme heterostructures. (E) Photocatalytic mechanism of Bi_2S_3-TCN heterojunctions.

further supported by the EIS data in Figure 4D (Xiao et al., 2022), in which the electric conductivity of Bi_2S_3-TCN with a minimal semi-circle is much better than Bi_2S_3 and TCN. Figures 4E,F show the Mott–Schottky plots for Bi_2S_3 and TCN, respectively. The positive slopes of the plots suggest that both materials are n-type semiconductors. The flat band potentials are found to be −0.74 and −0.43 V (vs RHE) for Bi_2S_3 and TCN, respectively, based on how the band alignment of the heterojunction is determined.

X-ray photoelectron spectroscopy (XPS) was utilized to analyze the chemical makeup and bonding structure of the final product. The shift in peak value demonstrated the transfer of electronic structure between TCN and Bi_2S_3. The XPS analysis identified the presence of Bi and S in Bi_2S_3, and C and N in TCN and Bi_2S_3-TCN, respectively. Supplementary Figures S1, S2 demonstrate a noteworthy decline in the binding energy direction of Bi_2S_3-TCN's C 1s and N 1s XPS peaks relative to TCN. Bi_2S_3-TCN's 2p and Bi 4f spectra also show a positive shift in binding energy (Supplementary Figure S3). The XPS spectra results indicate that there is

a close contact and charge transfer between Bi_2S_3 and TCN. We utilized the electron paramagnetic resonance (EPR) technique with 5,5-dimethyl-1-pyrroline N-oxide (DMPO) as the trapping agent of hydroxyl radical (•OH) (Figure 5A) to further confirm the charge transfer mechanism between Bi_2S_3 and TCN. Under visible light irradiation, four DMPO-•OH characteristic signal peaks with 1:2:2:1 intensity ratio of TCN and Bi_2S_3-TCN were observed, while no DMPO-•OH characteristic signal peaks appeared in Bi_2S_3. This indicates that the holes are concentrated in the VB of TCN and that only the VB level of TCN has sufficient oxidation capacity to reach •OH. Conversely, as shown in Figure 5B, the CB of both TCN and Bi_2S_3 is capable of reducing O_2 to •O_2^-, leading to the detection of the •O_2^- signal in all samples. Notably, the Bi_2S_3-TCN exhibits the most potent •O_2^- signal, which can be ascribed to the recombination between TCN's electrons and Bi_2S_3's holes, resulting in more electrons accumulating in the CB of Bi_2S_3. It is possible that the electrons on the CB of TCN transfer to the VB of Bi_2S_3, creating a Z-scheme heterojunction photocatalytic system, with higher oxidation and reduction capacities

located on TCN and Bi_2S_3, respectively. This suggests that photogenerated electrons and holes in Bi_2S_3-TCN may follow a Z-scheme electron transfer pattern instead of a type II electron transfer pattern (Supplementary Figure S4).

The work function (WF) of TCN, Bi_2S_3, and Bi_2S_3-TCN has been measured by Kelvin probe (Liu et al., 2022). The charge transfer direction in the composite photocatalyst can be well verified. As shown in Figure 5C, the contact potential difference (CPD) between TCN, Bi_2S_3, and Bi_2S_3-TCN and Au probes is 218 mV, 51 mV, and 130 mV, respectively, and the WF of TCN and Bi_2S_3 is calculated to be 5.29 and 5.12 eV, respectively (Figure 5D; Luo et al., 2023). When TCN and Bi_2S_3 are in contact, electrons are transferred from Bi_2S_3 to TCN through the contact interface until their Fermi levels reach equilibrium. This transfer method of electrons induces an embedded electric field between the positively charged Bi_2S_3 and negatively charged TCN at the interface. Consequently, carrier migration between Bi_2S_3 and TCN is accelerated. Within this particular embedded electric field, electrons accumulate at the TCN interface, while the electron density decreases at the Bi_2S_3 interface. This causes the TCN bands to bend downward and those on Bi_2S_3 to bend upward. Under illumination, the internal electric field and band bending facilitate the valence band transfer of conduction band electrons of tetracyanoquinodimethane to the boundary with Bi_2S_3, where they combine with the valence band hole of Bi_2S_3 to establish a Z-scheme electron transfer mechanism. This special charge transfer process accelerates the rate of carrier separation and transfer in the two components so that Bi_2S_3-TCN has a stronger REDOX capacity. As shown in Figure 5E, when both components in the heterojunction are excited under visible light radiation, the photocatalytic electrons in the CBM of TCN will diffuse and recombine with the electrons in the VBM of Bi_2S_3. With the formation of the S-scheme heterojunction, the high energy electrons in the CB of Bi_2S_3 and the high oxidative holes in the VB of TCN are retained (Liu et al., 2021). The participation of these highly active carriers in the following photocatalytic reactions are one important reason for the excellent photocatalytic hydrogen production of Bi_2S_3-TCN.

4 Conclusion

A green and environmentally benign route was adopted to successfully synthesize a Bi_2S_3-TCN heterojunction. The sample exhibits a 2D structure with a special surface morphology, and the intimate interface formed between Bi_2S_3 and TCN not only increases the photocatalytic charge separation efficiency but also extends the visible light adsorption of the sample, leading to a Z-scheme heterojunction with excellent photocatalytic performance. Bi_2S_3-TCN exhibits a hydrogen production rate of 65.2 $\mu mol\ h^{-1}$, which is 11.64 and 2.43 times those of Bi_2S_3 and TCN.

Data availability statement

The original contributions presented in the study are included in the article/Supplementary Material; further inquiries can be directed to the corresponding authors.

Author contributions

LY: Formal Analysis, Investigation, Software, Validation, Writing–original draft. YY: Data curation, Methodology, Writing–review and editing. PX: Data curation, Writing–original draft. YS: Data curation, Formal Analysis, Writing–review and editing. JG: Data curation, Formal Analysis, Writing–review and editing. JL: Data curation, Supervision, Writing–review and editing. HM: Data curation, Formal Analysis, Writing–review and editing. LL: Data curation, Investigation, Writing–original draft. YX: Data curation, Supervision, Writing–original draft. XX: Data curation, Funding acquisition, Writing–original draft. BJ: Data curation, Writing–original draft.

Funding

Conflict of interest

The authors declare that the research was conducted in the absence of any commercial or financial relationships that could be construed as a potential conflict of interest.

Publisher's note

Supplementary material

The Supplementary Material for this article can be found online at: https://www.frontiersin.org/articles/10.3389/fchem.2024.1340955/full#supplementary-material

References

Cao, S. W., Low, J. X., Yu, J. G., and Jaroniec, M. (2015). Polymeric photocatalysts based on graphitic carbon nitride. *Adv. Mat.* 27 (13), 2150–2176. doi:10.1002/adma.201500033

Chen, D. D., Fang, J. Z., Lu, S. Y., Zhou, G. Y., Feng, W. H., Yang, F., et al. (2017). Fabrication of Bi modified Bi_2S_3 pillared g-C_3N_4 photocatalyst and its efficient photocatalytic reduction and oxidation performances. *Appl. Surf. Sci.* 426, 427–436. doi:10.1016/j.apsusc.2017.07.13

Chen, J., Shen, S., Guo, P., Wang, M., Wu, P., Wang, X., et al. (2014). In-situ reduction synthesis of nano-sized Cu_2O particles modifying g-C_3N_4 for enhanced photocatalytic hydrogen production. *Appl. Catal. B* 152-153, 335–341. doi:10.1016/j.apcatb.2014.01.04

Cheng, L., Zhang, H. W., Li, X., Fan, J. J., and Xiang, Q. J. (2021). Carbon-graphitic carbon nitride hybrids for heterogeneous photocatalysis. *Small* 17 (1), 2005231. doi:10.1002/smll.202005231

Chu, S., Wang, Y., Guo, Y., Feng, J., Wang, C., Luo, W., et al. (2013). Band structure engineering of carbon nitride: in search of a polymer photocatalyst with high photooxidation property. *ACS Catal.* 3 (5), 912–919. doi:10.1021/cs4000624

Gu, J. Y., Yu, Y. L., Chen, S. W., Shi, W. C., Wang, Y. M., Liao, Y., et al. (2021). Heterojunction photocatalyst of cavity shaped Bi2S3/g-C3N4 for bisphenol a degradation: regulation of internal electric field via assistance of interfacial functional groups. *Chem. Eng. J.* 424, 130539. doi:10.1016/j.cej.2021.130539

Guo, R. T., Liu, X. Y., Qin, H., Wang, Z. Y., Shi, X., Pan, W. G., et al. (2020). Photocatalytic reduction of CO_2 into CO over nanostructure Bi_2S_3 quantum dots/ g-C_3N_4 composites with Z-scheme mechanism. *Appl. Surf. Sci.* 500, 144059. doi:10.1016/j.apsusc.2019.144059

Hao, Q., Xie, C. A., Huang, Y. M., Chen, D. M., Liu, Y. W., Wei, W., et al. (2020). Accelerated separation of photogenerated charge carriers and enhanced photocatalytic performance of g-C_3N_4 by Bi_2S_3 nanoparticles. *Chin. J. Catal.* 41, 249–258.

Hu, T. P., Dai, K., Zhang, J. F., Zhu, G. P., and Liang, C. H. (2019). One-pot synthesis of step-scheme Bi_2S_3/porous g-C_3N_4 heterostructure for enhanced photocatalytic performance. *Mater. Lett.* 257, 126740. doi:10.1016/j.matlet.2019.126740

Huang, Y., Mei, F., Zhang, J., Dai, K., and Dawson, G. (2022). Construction of 1D/2D $W_{18}O_{49}$/porous g-C_3N_4 S-scheme heterojunction with enhanced photocatalytic H_2 evolution. *Acta Physico-Chimica Sin.* 38 (7), 2108028. doi:10.3866/PKU.WHXB202108028

Kumar, R., Raizada, P., Verma, N., Hosseini-Bandegharaei, A., Thakur, V. K., Le, Q. V., et al. (2021). Recent advances on water disinfection using bismuth based modified photocatalysts: strategies and challenges. *J. Clean. Prod.* 297, 126617. doi:10.1016/j.jclepro.2021.126617

Kumar, S., Surendar, T., Baruah, A., and Shanker, V. (2013). Synthesis of a novel and stable g-C_3N_4–Ag_3PO_4 hybrid nanocomposite photocatalyst and study of the photocatalytic activity under visible light irradiation. *J. Mat. Chem. A* 1 (17), 5333–5340. doi:10.1039/C3TA00186E

Lee, W. P. C., Kong, X. Y., Tan, L. L., Gui, M. M., Sumathid, S., and Chai, S. P. (2018). Molybdenum disulfide quantum dots decorated bismuth sulfide as a superior noble-metal-free photocatalyst for hydrogen evolution through harnessing a broad solar spectrum. *Appl. Catal. B* 232, 117–123. doi:10.1016/j.apcatb.2018.03.019

Lei, Z., Ma, X., Hu, X., Fan, J., and Liu, E. (2022). Enhancement of photocatalytic H_2- evolution kinetics through the dual cocatalyst activity of Ni_2P-NiS-Decorated g-C_3N_4 heterojunctions. *Acta Physico-Chimica Sin.* 38 (7), 2110049. doi:10.3866/PKU.WHXB202110049

Li, Q., Jiao, Y., Tang, Y., Zhou, J., Wu, B., Jiang, B., et al. (2023b). Shear stress triggers ultrathin-nanosheet carbon nitride assembly for photocatalytic H2O2 production coupled with selective alcohol oxidation. *J. Am. Chem. Soc.* 145, 20837. doi:10.1021/jacs.3c05234

Li, Q., Meng, H., Zhou, P., Zheng, Y. Q., Wang, J., Yu, J. G., et al. (2013). Zn1-xCdxS solid solutions with controlled bandgap and enhanced visible-light photocatalytic H_2- production activity. *ACS Catal.* 3 (5), 882–889. doi:10.1021/cs4000975

Li, Q., Zhang, L., Liu, J., Zhou, J., Jiao, Y., Xiao, X., et al. (2021). Porous carbon nitride thin strip: precise carbon doping regulating delocalized π-electron induces elevated photocatalytic hydrogen evolution. *Small* 17, 2006622. doi:10.1002/smll.202006622

Li, Y., Liu, X. M., Tan, L., Cui, Z. D., Jing, D. D., Yang, X. J., et al. (2019). Eradicating multidrug-resistant bacteria rapidly using a multi functional g-C3N4@ Bi2S3 nanorod heterojunction with or without antibiotics. *Adv. Funct. Mat.* 29 (20), 1900946. doi:10.1002/adfm.201900946

Li, Y., Zhong, J., and Li, J. (2022). Rich carbon vacancies facilitated solar light-driven photocatalytic hydrogen generation over g- C_3N_4 treated in H_2 atmosphere. *Int. J. Hydrogen Energy.* 47 (94), 39886–39897. doi:10.1016/j.ijhydene.2022.09.147

Li, Y. M., Rao, F. Y., Zhong, J. B., and Li, J. Z. (2023a). In-situ fabrication of Bi2S3/ g-C3N4 heterojunctions with boosted H2 production rate under visible light irradiation. *Fuel* 341, 127629. doi:10.1016/j.fuel.2023.127629

Liu, J., Li, Q., Xiao, X., Li, F., Zhao, C., Sun, Q., et al. (2021). Metal-organic frameworks loaded on phosphorus-doped tubular carbon nitride for enhanced photocatalytic hydrogen production and amine oxidation. *J. Colloid Interface Sci.* 590, 1. doi:10.1016/j.jcis.2021.01.031

Liu, J., Sun, X., Jiang, B., Liu, M., Li, Q., Xiao, X., et al. (2022). UiO-66-NH_2 octahedral nanocrystals decorated with $ZnFe_2O_4$ nanoparticles for photocatalytic alcohol oxidation. *ACS Appl. Nano Mat.* 5, 2231. doi:10.1021/acsanm.1c03924

Liu, S. Q., Liu, Y. Y., Dai, G. P., Bao, X. Q., Huang, N., Peng, R., et al. (2019). Synthesis and characterization of novel Bi_2S_3/BiOCl/g-C_3N_4 composite with efficient visible-light photocatalytic activity. *Mat. Lett.* 241, 190–193. doi:10.1016/j.matlet.2019.01.087

Luo, F., Liu, M., Zheng, M., Li, Q., Wang, H., Zhou, J., et al. (2023). Boosted charge separation in direct Z-scheme heterojunctions of $CsPbBr_3$/Ultrathin carbon nitride for improved photocatalytic CO_2 reduction. *J. Mat. Chem.* 11, 241. doi:10.1039/d2ta07965h

Mua, F. H., Dai, B. L., Zhao, W., Yang, X. F., Zhao, X. L., and Guo, X. J. (2021). In-situ construction of amorphous/crystalline contact Bi_2S_3/Bi_4O_7 heterostructures for enhanced visible-light photocatalysis. *Chin. Chem. Lett.* 32, 2539–2543. doi:10.1016/j.cclet.2020.12.016

Okab, A. A., and Alwared, A. I. (2023). A dual S-scheme g-C_3N_4/Fe_3O_4/Bi_2WO_6/Bi_2S_3 heterojunction for improved photocatalytic decomposition of methylene blue: proposed mechanism, and stability studies. *Mater Sci. Semicond. Process* 153, 107196. doi:10.1016/j.mssp.2022.107196

Pan, H., Zhang, Y.-W., Shenoy, V. B., and Gao, H. (2011). *Ab initio* study on a novel photocatalyst: functionalized graphitic carbon nitride nanotube. *ACS Catal.* 1 (2), 99–104. doi:10.1021/cs100045u

Sarkar, P., De, S., and Neogi, S. (2022). Microwave assisted facile fabrication of dual Z-scheme g-C3N4/ZnFe2O4/Bi2S3 photocatalyst for peroxymonosulphate mediated degradation of 2,4,6-Trichlorophenol: the mechanistic insights. *Appl. Catal. B Environ.* 307, 121165. doi:10.1016/j.apcatb.2022.121165

Sun, J. W., Yang, S. R., Liang, Z. Q., Liu, X., Qiu, P. Y., Cui, H. Z., et al. (2020). Two-dimensional/one-dimensional molybdenum sulfide (MoS_2) nanoflake/graphitic carbon nitride (g-C_3N_4) hollow nanotube photocatalyst for enhanced photocatalytic hydrogen production activity. *J. Colloid Interface Sci.* 567, 300–307. doi:10.1016/j.jcis.2020.02.029

Thomas, A., Fischer, A., Goettmann, F., Antonietti, M., Müller, J.-O., Schlögl, R., et al. (2008). Graphitic carbon nitride materials: variation of structure and morphology and their use as metal-free catalysts. *J. Mat. Chem.* 18 (41), 4893–4908. doi:10.1039/B800274F

Wang, W., Zhang, H., Chen, Y., and Shi, H. (2022). Efficient degradation of tetracycline via coupling of photocatalysis and photo-fenton processes over a 2D/2D α-Fe_2O_3/g-C_3N_4 S-scheme heterojunction catalyst. *Acta Physico-Chimica Sin.* 38 (7), 2201008. doi:10.3866/PKU.WHXB202201008

Xiao, X., Lin, S., Zhang, L., Meng, H., Zhou, J., Li, Q., et al. (2021). Constructing Pd-N interactions in Pd/g-C3N4 to improve the charge dynamics for efficient photocatalytic hydrogen evolution. *Nano Res.* 15, 2928. doi:10.1007/s12274-021-3905-y

Xiao, X., Ruan, Z., Li, Q., Zhang, L., Meng, H., Zhang, Q., et al. (2022). A unique Fe–N_4 coordination system enabling transformation of oxygen into superoxide for photocatalytic C-H activation with high efficiency and selectivity. *Adv. Mat.* 34, 2200612. doi:10.1002/adma.202200612

Yin, J., Wu, Z. Y., Fang, M., Xu, Y., Zhu, W. J., and Li, C. (2018). *In situ* synthesis of C3N4/Bi2S3 composites with enhanced photocatalytic degradation performance under visible light irradiation. *J. Chin. Chem. Soc.* 65 (9), 1044–1052. doi:10.1002/jccs.201800002

Yuan, Y.-J., Chen, D., Yu, Z.-T., and Zou, Z.-G. (2018). Cadmium sulfide-based nanomaterials for photocatalytic hydrogen production. *J. Mat. Chem. A* 6 (25), 11606–11630. doi:10.1039/C8TA00671G

Zhang, J., Chen, X., Takanabe, K., Maeda, K., Domen, K., Epping, J. D., et al. (2010). Synthesis of a carbon nitride structure for visible-light catalysis by copolymerization. *Angew. Chem. Int. Ed.* 49 (2), 441–444. doi:10.1002/anie.200903886

Zhang, J., Sun, J., Maeda, K., Domen, K., Liu, P., Antonietti, M., et al. (2011a). Sulfur-mediated synthesis of carbon nitride: band-gap engineering and improved functions for photocatalysis. *Energy Environ. Sci.* 4 (3), 675–678. doi:10.1039/C0EE00418A

Zhang, J., Yu, J. G., Zhang, Y. M., Li, Q., and Gong, J. R. (2011b). Visible light photocatalytic H_2-production activity of CuS/ZnS porous nanosheets based on photoinduced interfacial charge transfer. *Nano Lett.* 11 (11), 4774–4779. doi:10.1021/nl202587b

Zhou, X., Yao, S. Y., Long, Y. M., Wang, Z. S., and Li, W. F. (2015). Microwave-assisted synthesis and enhanced visible-light-driven photocatalytic property of g-C_3N_4/ Bi_2S_3 nanocomposite. *Mat. Lett.* 145, 23. doi:10.1016/j.matlet.2015.01.084

Zhu, Q., Xu, Q., Du, M., Zeng, X., Zhong, G., Qiu, B., et al. (2022). Recent progress of metal sulfide photocatalysts for solar energy conversion. *Adv. Mat.* 34 (45), 2202929. doi:10.1002/adma.202202929